

Frontiers of Information Technology & Electronic Engineering
www.jzus.zju.edu.cn; engineering.cae.cn; www.springerlink.com
ISSN 2095-9184 (print); ISSN 2095-9230 (online)
E-mail: jzus@zju.edu.cn



OTFS modulation performance in a satellite-to-ground channel at sub-6-GHz and millimeter-wave bands with high mobility*

Tianshi LI¹, Ruisi HE^{†1}, Bo AI¹, Mi YANG¹, Zhangdui ZHONG¹, Haoxiang ZHANG^{‡2}

¹State Key Laboratory of Rail Traffic Control and Safety, Beijing Jiaotong University, Beijing 100044, China

²China Academy of Industrial Internet, Ministry of Industry and Information Technology, Beijing 100804, China

E-mail: 19125026@bjtu.edu.cn; ruisi.he@bjtu.edu.cn; boai@bjtu.edu.cn;

17111030@bjtu.edu.cn; zhdzhong@bjtu.edu.cn; zhx61778294@126.com

Received Sept. 10, 2020; Revision accepted Jan. 6, 2021; Crosschecked Feb. 4, 2021

Abstract: Orthogonal time frequency space (OTFS) modulation has been widely considered for high-mobility scenarios. Satellite-to-ground communications have recently received much attention as a typical high-mobility scenario and face great challenges due to the high Doppler shift. To enable reliable communications and high spectral efficiency in satellite mobile communications, we evaluate OTFS modulation performance for geostationary Earth orbit and low Earth orbit satellite-to-ground channels at sub-6-GHz and millimeter-wave bands in both line-of-sight and non-line-of-sight cases. The minimum mean squared error with successive detection (MMSE-SD) is used to improve the bit error rate performance. The adaptability of OTFS and the signal detection technologies in satellite-to-ground channels are analyzed. Simulation results confirm the feasibility of applying OTFS modulation to satellite-to-ground communications with high mobility. Because full diversity in the delay-Doppler domain can be explored, different terminal movement velocities do not have a significant impact on the performance of OTFS modulation, and OTFS modulation can achieve better performance compared with classical orthogonal frequency division multiplexing in satellite-to-ground channels. It is found that MMSE-SD can improve the performance of OTFS modulation compared with an MMSE equalizer.


Key words: Delay-Doppler channel; High-mobility communications; Minimum mean squared error with successive detection (MMSE-SD); Orthogonal time frequency space (OTFS); Satellite-to-ground communications; Millimeter-wave communications

<https://doi.org/10.1631/FITEE.2000468>

CLC number: TN92

[‡] Corresponding authors

* Project supported by the National Key R&D Program of China (No. 2020YFB1806903), the National Natural Science Foundation of China (Nos. 61922012, 62001519, 52042201, U1834210, and 61961130391), the State Key Laboratory of Rail Traffic Control and Safety, China (Nos. RCS2020ZT008, RCS2019ZZ007, and RCS2020ZT010), the Teaching Reform Project, China (No. 134811522), and the Fundamental Research Funds for the Central Universities, China (Nos. 2020JBZD005 and I20JB0200030)

 ORCID: Tianshi LI, <https://orcid.org/0000-0001-8287-0576>; Ruisi HE, <https://orcid.org/0000-0003-4135-3227>; Bo AI, <https://orcid.org/0000-0001-6850-0595>; Zhangdui ZHONG, <https://orcid.org/0000-0001-8889-7374>

© Zhejiang University Press 2021

1 Introduction

Future communication systems such as beyond fifth generation (B5G) and sixth generation (6G) systems are supposed to support high data rates in high-mobility scenarios, such as vehicle-to-vehicle (V2V) communications (He et al., 2020), high-speed railway communications (Ai et al., 2020), millimeter-wave mobile-to-mobile (M2M) communications (He et al., 2018), and satellite-to-ground mobile communications (Jayaprakash et al., 2019). In these scenarios,

communication systems face great challenges due to the time-varying channels and high Doppler shift. Therefore, it is important to achieve reliable and efficient communications in high-mobility scenarios with high Doppler shift. Moreover, B5G and 6G communication systems are expected to provide seamless global coverage. To meet this requirement, non-terrestrial networks (NTNs), such as inter-satellite communications (Lin et al., 2020) and unmanned aerial vehicle (UAV) communications (Fan et al., 2020), need to be used to complement current communication systems (You et al., 2020). Due to the high latency and high Doppler shift in satellite-to-ground communications, the orthogonal frequency division multiplexing (OFDM) based system faces great challenges in estimating and compensating for the Doppler shift, and the performance suffers from serious degradation because of the inter-carrier interference (ICI) (Wang et al., 2006). Therefore, classical OFDM cannot meet the needs of satellite-to-ground high-mobility communications.

Orthogonal time frequency space (OTFS) modulation was proposed as a modulation technology for high-mobility scenarios (Hadani et al., 2017). By placing symbols in the delay-Doppler domain, OTFS modulation can almost change the rapid time-varying channel into a non-fading channel. OTFS modulation fully exploits the time and frequency diversity, which makes it robust when combating high Doppler shift. The full diversity also enables OTFS modulation to achieve further performance improvement compared with OFDM in fast time-varying channels (Surabhi et al., 2019). In Nimr et al. (2018), Raviteja et al. (2018), and Surabhi et al. (2019), it has been shown that OTFS modulation has significant advantages compared with OFDM in some high-mobility scenarios.

Another reason for the extraordinary performance of the OTFS technique is that it can achieve channel hardening even in a single-input single-output system (Hadani et al., 2018). In other words, OTFS modulation can achieve channel hardening as a MIMO system without the phenomenon of mutual antenna coupling in a MIMO system (Chen XM et al., 2018). OTFS system is similar to OFDM orbital angular momentum (OAM) system where they both use two-dimensional channel resources to transmit signals, which can improve spectral efficiency and channel capacity (Chen R et al., 2018; Chen

XM et al., 2020). It has shown significantly robust OTFS performance in some high-mobility channel models, such as the extended vehicular A (EVA) channel model (Raviteja et al., 2019b), WINNER II model (Shen et al., 2019), and 5G tapped delay line (TDL) based channel model (Zhang et al., 2019). However, the performance of OTFS modulation in satellite-to-ground high-mobility communications has not been well analyzed. To evaluate the feasibility of OTFS modulation in satellite-to-ground communications, it is necessary to analyze its performance using satellite-to-ground channel models with high mobility.

In high-mobility scenarios, each data symbol in the delay-Doppler domain is subject to interference from its neighboring symbols due to multipath propagation and the Doppler effect, and the performance of OTFS modulation will degrade because of the interference. Therefore, OTFS modulation performance is closely related to the signal detection technology. Linear equalization methods, such as the minimum mean squared error (MMSE), are widely adopted to recover signals. However, simulation results in Hadani et al. (2018) and Pfadler et al. (2020) show that MMSE may perform poorly because of the lack of interference cancellation. To improve the performance of the OTFS system, MMSE with successive detection (MMSE-SD) technology (Choi et al., 2001) is adopted, which can reduce the interference of the already detected data symbols on other data symbols. Moreover, the adaptability of the MMSE method in satellite-to-ground communications for OTFS signal detection has not been well analyzed. Therefore, further investigation of OTFS signal detection is needed.

To fill in the above mentioned gaps, we apply OTFS modulation to satellite-to-ground high-mobility communications and evaluate the performance of OTFS and OFDM modulations using the recently developed 5G NTN-TDL-based channel model (3GPP, 2020). The MMSE-SD technology is used to improve the OTFS bit error rate (BER) performance. The results of this study are useful in testing the feasibility of OTFS modulation in satellite-to-ground communications. Moreover, in this study, we demonstrate better performance of MMSE-SD compared with MMSE in high-mobility scenarios through simulations.

2 Orthogonal time frequency space system

In this section, the OTFS system is briefly introduced. Specifically, we first introduce the characteristics of wireless channels in the delay-Doppler domain. Then, the signal processing scheme of OTFS is presented.

2.1 Delay-Doppler domain channel

The time-frequency channel can be divided into $M \times N$ grids, which can be expressed as

$$\gamma = \{(m\Delta f, nT), m = 0, 1, \dots, M-1, n = 0, 1, \dots, N-1\}, \quad (1)$$

where Δf (Hz) and T (s) represent the sampling intervals on the frequency axis and time axis, respectively. Parameters n and m denote the indexes of the grids on the time axis and frequency axis, respectively. Therefore, the transmission bandwidth of the OTFS system is $B = M\Delta f$, and the transmission duration is $T_d = NT$.

The Doppler channel corresponding to the time-frequency channel can be expressed as

$$\Gamma = \left\{ \left(\frac{l}{M\Delta f}, \frac{k}{NT} \right), l = 0, 1, \dots, M-1, k = 0, 1, \dots, N-1 \right\}. \quad (2)$$

$f_r = 1/(NT)$ and $d_r = 1/(M\Delta f)$ represent the sampling intervals on the Doppler axis and delay axis, respectively, which can be regarded as the resolutions of the Doppler domain and delay domain, respectively. The resolution of the delay domain determines the ability of the OTFS system to recognize multipath components. Parameters k and l denote the indexes of the grids on the Doppler axis and delay axis, respectively.

The delay-Doppler domain channel impulse response $h(\tau, v)$ is a natural fit to the propagation physics (Hadani et al., 2017). Considering that the

delay-Doppler domain channel is sparse, the channel can be modeled as (Raviteja et al., 2019a)

$$h(\tau, v) = \sum_{i=1}^P h_i \delta(\tau - \tau_i) \delta(v - v_i), \quad (3)$$

where P is the path number, h_i denotes the complex channel gain, and τ_i and v_i represent the delay tap and Doppler tap of the i^{th} path, respectively. Because N and M are sufficiently large, we assume that the OTFS system can resolve all the paths in the channel. Therefore, τ_i and v_i are integer multiples of the delay domain resolution and Doppler domain resolution, respectively. The delay tap and Doppler tap of the i^{th} path can be expressed as

$$\tau_i = \frac{l_i}{M\Delta f}, v_i = \frac{k_i}{NT}, \quad (4)$$

where l_i is the index of τ_i on the delay axis and k_i is the index of v_i on the Doppler axis.

2.2 Signal processing scheme

We consider OTFS modulation using the OFDM-based OTFS model. It is a single-input single-out system without channel coding, as shown in Fig. 1. For ease of expression, the matrix form is used to describe the signal process scheme at the transmitter and the receiver (Hadani et al., 2017; Raviteja et al., 2019a). Let $\text{vec}(\cdot)$ and $\text{vec}^{-1}(\cdot)$ denote the matrix-to-vector conversion and the inverse operation, respectively, and “ \otimes ” denote the Kronecker product. Parameters \mathbf{F}_n and \mathbf{F}_n^H are the n -point discrete Fourier transform (DFT) and the inverse discrete Fourier transform (IDFT) matrices, respectively. Let $(\cdot)^H$ and $(\cdot)^T$ represent the Hermitian transpose and the transpose, respectively. Parameters \mathbf{G}_{tx} and \mathbf{G}_{rx} represent the waveform matrices at the transmitter and the receiver, respectively. By sampling the transmit pulse $g_{tx}(t)$ and the received pulse $g_{rx}(t)$, \mathbf{G}_{tx} and \mathbf{G}_{rx} can be obtained. For rectangular waveform, \mathbf{G}_{tx} and \mathbf{G}_{rx} equal the identity matrix.

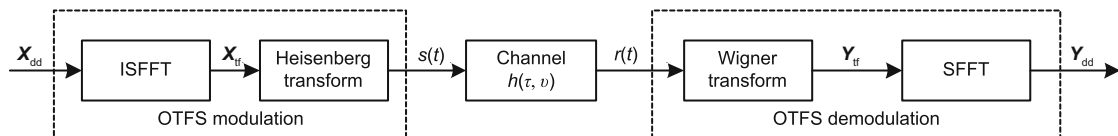


Fig. 1 Signal processing scheme of OTFS modulation

OTFS: orthogonal time frequency space; ISFFT: inverse symplectic finite Fourier transform; SFFT: symplectic finite Fourier transform

At the transmitter, let $\mathbf{x} \in \mathbb{C}^{MN \times 1}$ denote the quadrature amplitude modulation (QAM) symbols to be transmitted. First, place symbols on the delay-Doppler domain, i.e., $\mathbf{X}_{\text{dd}} = \text{vec}^{-1}(\mathbf{x})$, where $\mathbf{X}_{\text{dd}} \in \mathbb{C}^{M \times N}$. With the inverse symplectic finite Fourier transform (ISFFT), the signal can be transformed to the time-frequency domain, which can be expressed as

$$X[m, n] = \frac{1}{MN} \sum_{k=0}^{N-1} \sum_{l=0}^{M-1} x[l, k] e^{j2\pi(\frac{nk}{N} - \frac{ml}{M})}, \quad (5)$$

where $x[l, k]$ denotes the (l, k) th element of the signal \mathbf{X}_{dd} , and $X[m, n]$ denotes the (m, n) th element of the signal in the time-frequency domain $\mathbf{X}_{\text{tf}} \in \mathbb{C}^{M \times N}$. Signal \mathbf{X}_{tf} can be written as (Raviteja et al., 2019a)

$$\mathbf{X}_{\text{tf}} = \mathbf{F}_M \mathbf{X}_{\text{dd}} \mathbf{F}_N^H. \quad (6)$$

Next, using the Heisenberg transform, the time-frequency domain symbols $X[m, n]$ can be pulse-shaped and transmitted to the time domain. That is, signal \mathbf{X}_{tf} is transformed to the time-delay domain through the Heisenberg transform, which can be represented in a matrix form as $\mathbf{S} = \mathbf{G}_{\text{tx}} \mathbf{F}_M^H \mathbf{X}_{\text{tf}}$. After vectorization, the signal in the time domain can be expressed as

$$\begin{aligned} \mathbf{s} &= \text{vec}(\mathbf{S}) = \text{vec} \left(\mathbf{G}_{\text{tx}} \mathbf{X}_{\text{dd}} \mathbf{F}_N^H \right) \\ &= (\mathbf{F}_N^H \otimes \mathbf{G}_{\text{tx}}) \mathbf{x}, \end{aligned} \quad (7)$$

where $\mathbf{s} \in \mathbb{C}^{MN \times 1}$ is the sampling of the time-domain signal $s(t)$ with a sampling rate of $M\Delta f$.

At the receiver, the received baseband signal can be expressed as

$$r(t) = \sum_{i=1}^P h_i e^{j2\pi v_i(t-\tau_i)} s(t-\tau_i) + w(t). \quad (8)$$

After sampling the signal $r(t)$ at the rate of $M\Delta f$, the discrete baseband received signal vector $\mathbf{r} \in \mathbb{C}^{MN \times 1}$ can be obtained in a vectorized form:

$$\mathbf{r} = \mathbf{H} \mathbf{s} + \mathbf{w}. \quad (9)$$

To obtain the received time-frequency domain signal $\mathbf{Y}_{\text{tf}} \in \mathbb{C}^{M \times N}$, signal \mathbf{r} should first be reshaped into a matrix form with the size of $M \times N$, i.e., $\mathbf{R} = \text{vec}^{-1}(\mathbf{r})$. Then, signal \mathbf{Y}_{tf} can be derived using the Wigner transform (the inverse of Heisenberg transform) as $\mathbf{Y}_{\text{tf}} = \mathbf{F}_M \mathbf{G}_{\text{rx}} \mathbf{R}$.

Finally, after symplectic finite Fourier transform (SFFT) and vectorization, signal \mathbf{Y}_{tf} can be transformed to the delay-Doppler domain, which can be expressed as

$$\mathbf{Y}_{\text{dd}} = \mathbf{F}_M^H \mathbf{Y}_{\text{tf}} \mathbf{F}_N = \mathbf{G}_{\text{rx}} \mathbf{R} \mathbf{F}_N. \quad (10)$$

Using the property of $\text{vec}(\mathbf{ABC}) = (\mathbf{C}^T \otimes \mathbf{A}) \text{vec}(\mathbf{B})$ and $\mathbf{F}_N^T = \mathbf{F}_N$, signal \mathbf{y} can be expressed as

$$\begin{aligned} \mathbf{y} &= \text{vec}(\mathbf{Y}_{\text{dd}}) = (\mathbf{F}_N^T \otimes \mathbf{G}_{\text{rx}}) \mathbf{r} \\ &= (\mathbf{F}_N \otimes \mathbf{G}_{\text{rx}}) \mathbf{H} (\mathbf{F}_N^H \otimes \mathbf{G}_{\text{tx}}) \mathbf{x} + (\mathbf{F}_N \otimes \mathbf{G}_{\text{rx}}) \mathbf{w} \\ &= \mathbf{H}_{\text{eff}} \mathbf{x} + \mathbf{w}', \end{aligned} \quad (11)$$

where $\mathbf{H}_{\text{eff}} \in \mathbb{C}^{MN \times MN}$ denotes the effective delay-Doppler domain channel matrix, which can be used for channel equalization. Parameter \mathbf{w}' is the noise vector.

3 Channel estimation and equalization

For channel estimation, we consider the embedded pilot-aided channel estimation algorithm (Raviteja et al., 2019b). The pilot is placed in the delay-Doppler domain to probe the channel and is surrounded by guard intervals. The data symbols can be placed in other grids in the delay-Doppler domain, as shown in Fig. 2a. The delay-Doppler channel is divided into $M \times N$ grids, where $M = 32$ and $N = 32$. The impulse is a pilot that is sufficiently far away from the data symbols. The pilot experiences the same interaction with the channel as the data symbols. Through OTFS modulation, the signal in the delay-Doppler domain can be transformed to the delay-time domain, as shown in Fig. 2b. Each data symbol is assigned to each time tap in the time-delay domain. At the receiver, after recovering the signal to the delay-Doppler domain, the data symbols in the OTFS frame go through the entire time-varying channel. OTFS modulation can achieve time diversity due to the Doppler shift. Therefore, OTFS modulation can be more resistant to high Doppler shifts in the channel.

After OTFS demodulation, the received signal \mathbf{r} can be transformed to signal \mathbf{y} in the delay-Doppler domain. We use the MMSE algorithm for signal detection and the MMSE-SD algorithm to improve the BER performance of the OTFS system. For MMSE equalization, equalizer matrix \mathbf{G}_{MMSE} minimizes the

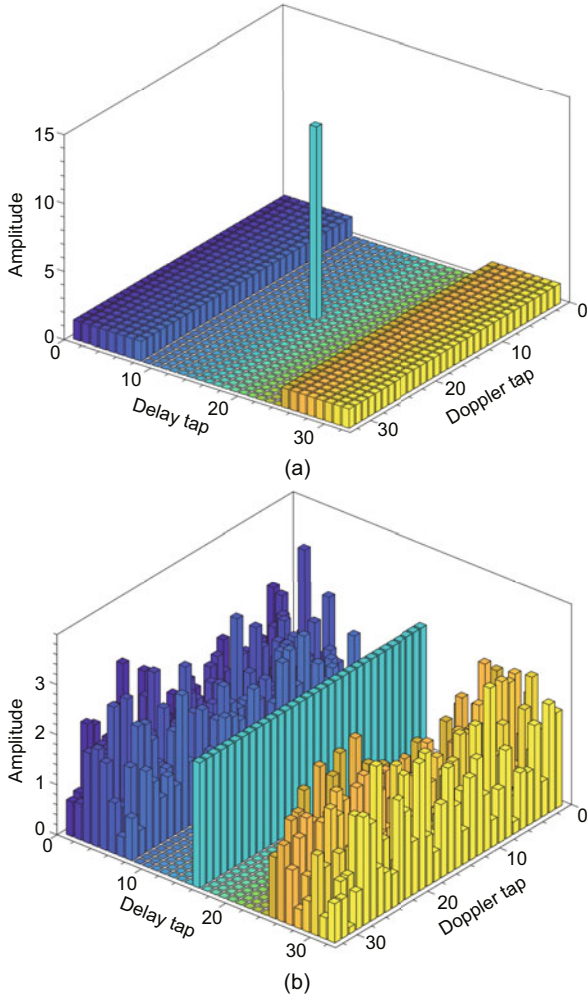


Fig. 2 Delay-Doppler domain signal X_{dd} (a) and time-delay domain signal S (b)

mean squared error between the estimated signal \hat{x} and the transmitted signal x . The output of the MMSE equalizer can be expressed as

$$\hat{x} = \mathbf{G}_{\text{MMSE}} \mathbf{y} = \left(\mathbf{H}_{\text{eff}}^H \mathbf{H}_{\text{eff}} + \sigma_w^2 \mathbf{I} \right)^{-1} \mathbf{H}_{\text{eff}}^H \mathbf{y}, \quad (12)$$

where $\mathbf{I} \in \mathbb{C}^{MN \times MN}$ is the identity matrix and σ_w^2 represents the noise variance.

The MMSE-SD algorithm is based on the MMSE method, which detects data symbols individually instead of detecting all the data symbols simultaneously (Choi et al., 2001). Using successive interference cancellation, the interference caused by the detected symbols can be suppressed, which reduces the interference in the received signal and improves the performance.

The detection order of data symbols has a significant impact on the detection performance. As long

as the current detected symbol is correct, there will be less interference in the next detection (Choi et al., 2001). MMSE-SD uses the post-detection signal-to-interference-and-noise ratio (SINR) to determine the detection order. The data symbol with a larger SINR is selected as the first detected data symbol. SINR of the k^{th} symbol of signal x can be expressed as

$$\text{SINR}_k = \frac{|\mathbf{g}_k \mathbf{h}_k|^2}{\sum_{j, j \neq k} |\mathbf{g}_k \mathbf{h}_j|^2 + \sigma_w^2 \|\mathbf{g}_k\|^2}, \quad (13)$$

where $\mathbf{g}_k = (\mathbf{G}_{\text{MMSE}})_k \in \mathbb{C}^{1 \times MN}$ represents the k^{th} row of \mathbf{G}_{MMSE} , and $\mathbf{h}_j = (\mathbf{H}_{\text{eff}})_j \in \mathbb{C}^{MN \times 1}$ represents the j^{th} column of \mathbf{H}_{eff} . $|\cdot|$ represents the absolute value of a scalar, and $\|\cdot\|$ represents the 2-norm of a vector. The detection order of data symbols is $\{l_1, l_2, \dots, l_{NM}\}$, where l_i ($i = 1, 2, \dots, NM$) denotes the index of the data symbol in x and can be determined as $l_i = \underset{k}{\text{argmax}} \text{SINR}_k$. The estimated data symbols are $\hat{x} = (\hat{x}_1, \hat{x}_2, \dots, \hat{x}_{NM})^T$.

The MMSE-SD algorithm steps are as follows: First, the l_i^{th} symbol of the original transmitted signal is estimated, i.e., $\hat{x}_{l_i} = \mathbf{g}_{l_i} \mathbf{y}$. According to the constellation, by making a hard decision on \hat{x}_{l_i} , the detected data symbol \hat{a}_{l_i} can be obtained. Assuming that \hat{a}_{l_i} is correct, this detected data symbol can be used to eliminate the interference on the remaining symbols of the received signal \mathbf{y} , i.e., $\mathbf{y}_{\text{new}} = \mathbf{y} - \hat{a}_{l_i} (\mathbf{H}_{\text{eff}})_{l_i}$. Next, \mathbf{H}_{eff} can be renewed by setting the l_i^{th} column of \mathbf{H}_{eff} to zero. Then, \mathbf{G}_{MMSE} can be updated using the new \mathbf{H}_{eff} . Repeat the above steps until all the data symbols are detected.

4 Simulation results and analysis

In this section, the performances of OTFS and OFDM modulation under different scenarios, line-of-sight (LoS) and non-line-of-sight (NLoS) conditions, different signal detection algorithms, and different Doppler shift conditions are investigated. Specifically, we first investigate the BER performance of OTFS modulation and compare it with that of OFDM in different scenarios. Next, we investigate the impact of different signal detection algorithms on OTFS BER performance.

4.1 Simulation parameters

The satellite-to-ground mobile channel models (3GPP, 2020) are adopted, where the tapped delay line (TDL) models are defined for the S (2 GHz) and Ka (DL 20 GHz, UL 30 GHz) bands. The NTN-TDL-B model is constructed to represent NLoS conditions, and the NTN-TDL-C model is constructed to represent LoS conditions in 3GPP TR 38.811. Both models are applicable to S and Ka bands, and can be applied in different environments, including urban, dense urban, suburban, and rural scenarios. Different communication scenarios generally have different channel parameters, such as root mean square (RMS) delay spread in taps and K -factors, and details of the channel model are presented (3GPP, 2020).

In this study, BER performances of OTFS modulation in urban, dense urban, suburban, and rural scenarios are evaluated. The NTN-TDL-B and NTN-TDL-C channel models are adopted to represent NLoS and LoS cases, respectively. The simulation parameters are listed in Table 1. The modulation type is 4-QAM and the transmitted data is uncoded.

4.2 Geostationary Earth orbit satellite-to-ground communications

The geostationary Earth orbit (GEO) satellite moves in a geosynchronous orbit and has the same speed as the Earth's rotation. Therefore, the GEO satellite appears to be stationary for the Earth, and in this condition, the Doppler frequency shift is caused mainly by the terminal movement. In simulations, we set the moving velocities of the terminal to 350, 500, and 1000 km/h. The Doppler shift can be expressed as (Li et al., 2012)

$$f_d = f_c \frac{v_t \cos \theta}{c} = \frac{f_c v_t (R_e + l_s) \sin \varphi}{c \sqrt{2R_e(R_e + l_s)(1 - \cos \varphi) + l_s^2}}, \quad (14)$$

Table 1 Simulation parameters

Parameter	Value
OTFS frame size (M, N)	(128, 32)
Subcarrier spacing (kHz)	15
Modulation type	4-QAM
Bandwidth (MHz)	1.92
Frame duration (s)	0.002 13
Doppler resolution (Hz)	$f_r = 1/(NT) = 468.75$
Delay resolution (ns)	$d_r = 1/(M\Delta f) = 520.8$

where φ is the angle between the straight line from the center of the Earth to the terminal and satellite. Parameter R_e is the radius of the Earth, which is 6370 km. Parameter l_s denotes the orbit height of the satellite. The terminal has a velocity of v_t , f_c is the carrier frequency, and c is the velocity of light. When $\varphi = 40^\circ$, $l_s = 35\,800$ km, and $f_c = 2.2$ GHz, the maximum Doppler shifts caused by the terminal's motion are about 515, 736, and 1475 Hz, respectively.

Fig. 3 shows the BER performances of OTFS and OFDM modulations with different Doppler frequencies using MMSE equalization, where the NTN-TDL-C model is adopted to represent the LoS case. The urban scenario is considered and the subcarrier spacing is 15 kHz. For OTFS modulation, it is observed that a BER of 10^{-4} is realized when SNR is about 17 dB for the three velocity cases, whereas at the same SNR, the OTFS modulation BER is almost invariant to the Doppler shift and is close to 10^{-4} . For OFDM modulation, the BER increases significantly with the increase of the Doppler shift. The high Doppler shift causes severe ICI, which results in significant degradation of OFDM BER performance. Compared with OFDM, OTFS modulation has better resistance to high Doppler shift because the full time and frequency diversity can be exploited. Fig. 3 illustrates the robustness of OTFS modulation in GEO satellite-to-ground channels with high moving velocity of the terminal.

In Figs. 4 and 5, we compare the BER performances of OTFS and OFDM modulations under

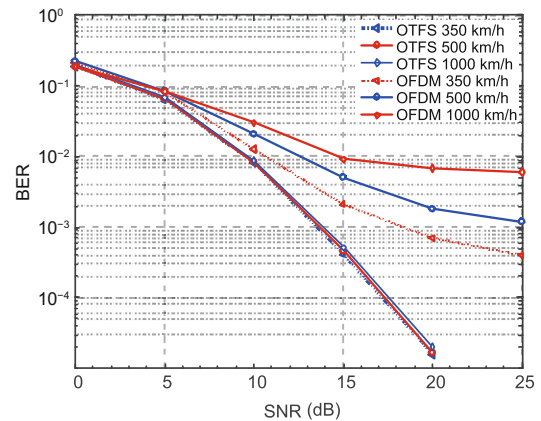


Fig. 3 BER performance of OTFS and OFDM for three different velocities, i.e., 350, 500, and 1000 km/h, in a GEO satellite-to-ground channel

BER: bit error rate; OTFS: orthogonal time frequency space; OFDM: orthogonal frequency division multiplexing; GEO: geostationary Earth orbit

four different scenarios (dense urban, urban, suburban, and rural) in LoS and NLoS conditions using MMSE equalization. The NTN-TDL-C and NTN-TDL-B channel models are used to represent the LoS and NLoS cases, respectively. The terminal's velocity is 500 km/h, and the carrier frequency is 2.2 GHz. It is found that for all scenarios, OTFS modulation achieves considerable improvement compared with OFDM because OTFS modulation has better resistance to high Doppler shift; the performance improvement is about 15 dB. In the LoS case, the BER performances of both OTFS and OFDM modulations in the suburban scenario are generally the best. The performances of OTFS modulation in dense urban, urban, and rural scenarios are similar. This is because the K -factor of the channel model used in the suburban scenario is much higher than those in three other scenarios, whereas the dense urban, urban, and rural scenarios generally have similar delay spreads and K -factors in the 3GPP channel model. In the NLoS case, the scenario's impact on the BER is relatively small (Fig. 5), because in the 3GPP channel model, the NLoS channel parameters are generally close to each other for different scenarios, and only the dense urban scenario has a larger RMS delay spread, thus a higher BER (Fig. 5).

In Fig. 6, we compare the BER performances of MMSE and MMSE-SD for OTFS modulation. The NTN-TDL-B channel is selected, and the urban scenario is considered. The carrier frequencies are 2.2

and 20 GHz, and the terminal's velocity is 500 km/h. The subcarrier spacings are 15 and 60 kHz, corresponding to the carrier frequencies of 2.2 and 20 GHz, respectively. For MMSE equalization, a BER performance of 10^{-4} can be obtained at an SNR of 20 dB, whereas for the MMSE-SD algorithm, a BER of 10^{-4} can be obtained when the SNR is about 17.5 dB. This shows that the MMSE-SD algorithm achieves about 2.5 dB gain compared with the MMSE equalizer. This is because the MMSE-SD algorithm detects the symbols one by one. Using successive interference cancellation, the interference from the detected symbols can be eliminated. The above results prove that using the MMSE-SD algorithm can effectively

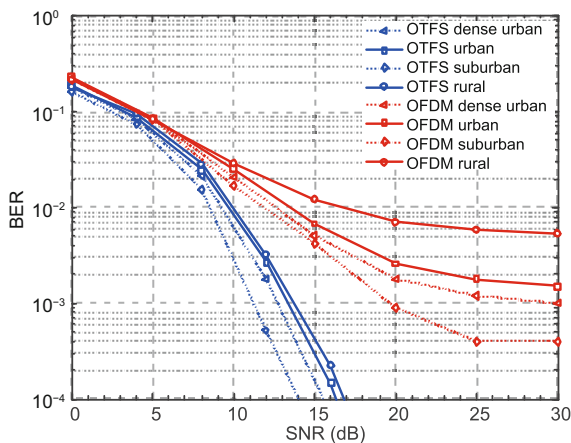


Fig. 4 BER performance of OTFS and OFDM in a GEO satellite-to-ground channel in dense urban, urban, suburban, and rural scenarios, under LoS conditions

BER: bit error rate; OTFS: orthogonal time frequency space; OFDM: orthogonal frequency division multiplexing; GEO: geostationary Earth orbit; LoS: line-of-sight

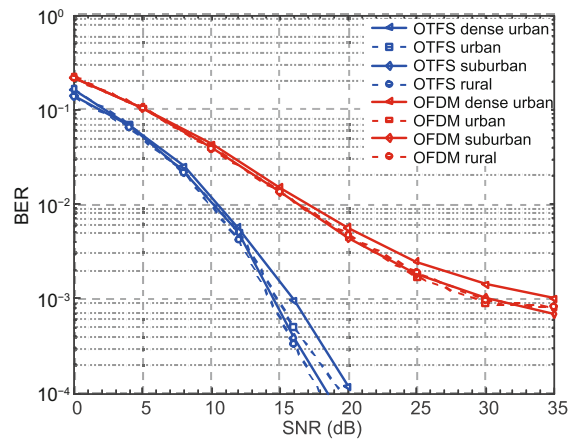


Fig. 5 BER performance of OTFS and OFDM in a GEO satellite-to-ground channel in dense urban, urban, suburban, and rural scenarios, under NLoS conditions

BER: bit error rate; OTFS: orthogonal time frequency space; OFDM: orthogonal frequency division multiplexing; GEO: geostationary Earth orbit; NLoS: non-line-of-sight

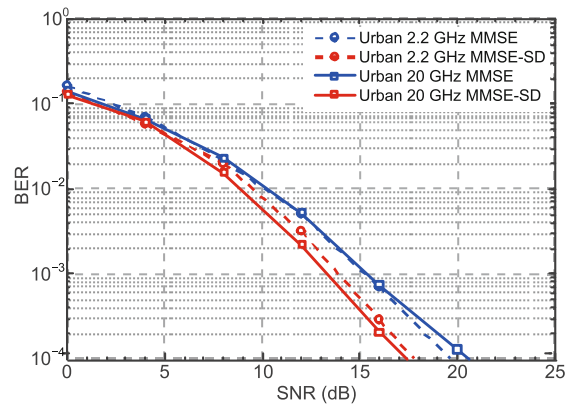


Fig. 6 BER performance comparison of MMSE and MMSE-SD in the NLoS condition for OTFS

BER: bit error rate; MMSE: minimum mean squared error; MMSE-SD: MMSE with successive detection; NLoS: non-line-of-sight; OTFS: orthogonal time frequency space

improve the BER performance of OTFS modulation in GEO satellite-to-ground mobile communications compared with the MMSE equalizer.

4.3 Low Earth orbit satellite-to-ground communications

For a non-GEO satellite, the Doppler effect is caused by the motion of both the satellite and the terminal. When the terminal is not moving, all paths arriving at the satellite exhibit the same Doppler shift because of the high altitude of satellite (Papathanassiou et al., 2001). In general, the Doppler shift caused by the motion of satellites can be pre-compensated for because the motion of satellites follows known paths. The velocity of a low Earth orbit (LEO) satellite at 1500-km altitude is 7.1172 km/s. When the carrier frequencies are 2 and 20 GHz, the maximum Doppler shifts caused by the motion of the satellite are up to 40 and 400 kHz, respectively, and the carrier frequency shift caused by the satellite's movement should be considered (3GPP, 2020). Therefore, the Doppler shift caused by the terminal's motion is expressed as

$$f_d = (f_{d,\text{shift}} + f_c) \frac{v_t}{c} \cos \alpha \cos \psi, \quad (15)$$

where v_t denotes the terminal's velocity, ψ is the angle between the direction of the terminal's motion and the projected plane of the satellite, and α is the satellite's elevation angle. Parameter $f_{d,\text{shift}}$ denotes the frequency shift caused by the satellite's motion, which can be expressed as (3GPP, 2020)

$$f_{d,\text{shift}} = \frac{v_{\text{sat}}}{c} \frac{R_e}{R_e + l_s} f_c \cos \alpha, \quad (16)$$

where v_{sat} denotes the satellite's velocity.

For an LEO satellite-to-ground channel, the carrier frequencies of 2.2 and 20 GHz and the terminal velocities of 500 and 1000 km/h are considered. When $l_s = 1500$ km and $\alpha = 50^\circ$, for a carrier frequency of 2.2 GHz, the maximum Doppler shifts caused by the terminal's motion are 654 and 1310 Hz, corresponding to the velocities of 500 and 1000 km/h, respectively. For a carrier frequency of 20 GHz, the maximum Doppler shifts caused by the terminal's motion are about 5.9 and 11.9 kHz, corresponding to the velocities of 500 and 1000 km/h, respectively.

Figs. 7 and 8 show the performances of OTFS and OFDM modulations in the dense urban, urban,

suburban, and rural scenarios. The NTN-TDL-B and NTN-TDL-C channel models are used to represent the NLoS and LoS cases, respectively. The subcarrier spacing is 60 kHz, the terminal's velocity is 500 km/h, and the carrier frequency is 20 GHz. In the LoS conditions, OTFS modulation achieves a BER of 10^{-4} when SNR is about 16 dB in all scenarios. In the NLoS case, OTFS modulation achieves a BER of 10^{-4} at an SNR of 21 dB. It is shown that the performance gap between OTFS and OFDM modulations in NLoS conditions is larger than that in LoS conditions. In NLoS conditions, the main difference

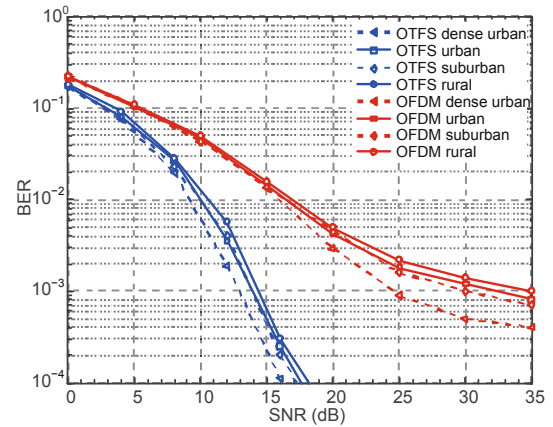


Fig. 7 BER performance of OTFS and OFDM in an LEO satellite-to-ground channel in dense urban, urban, suburban, and rural scenarios, under LoS conditions

BER: bit error rate; OTFS: orthogonal time frequency space; OFDM: orthogonal frequency division multiplexing; LEO: low Earth orbit; LoS: line-of-sight

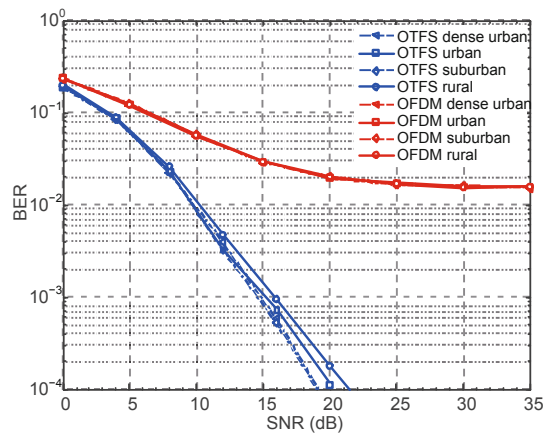


Fig. 8 BER performance of OTFS and OFDM in an LEO satellite-to-ground channel in dense urban, urban, suburban, and rural scenarios, under NLoS conditions

BER: bit error rate; OTFS: orthogonal time frequency space; OFDM: orthogonal frequency division multiplexing; LEO: low Earth orbit; NLoS: non-line-of-sight

in the channel model for the four scenarios is RMS delay spread. Because OTFS modulation can achieve full diversity in the delay domain, its performances are similar in all four scenarios. OFDM can also achieve full diversity in the delay domain when the subcarrier number M is sufficiently large. Therefore, scenarios do not significantly affect the performances of OTFS and OFDM modulations in the NLoS case.

In Figs. 9 and 10, the BER performances with MMSE-SD and MMSE for different velocities and carrier frequencies are presented. The NTN-TDL-B model is used, and the dense urban scenario is considered. The subcarrier spacings are 15 and 60 kHz for 2.2 and 20 GHz, respectively, and the terminal has velocities of 500 and 1000 km/h. For different terminal velocities and carrier frequencies, MMSE-SD achieves about 2.3-dB gain compared with MMSE, at a BER of 10^{-4} . Using symbol cancellation, interference caused by the detected symbols can be subtracted from the received signal \mathbf{y} , resulting in less interference in the received signal. The results demonstrate better performance for MMSE-SD compared with MMSE in LEO satellite-to-ground communications with high mobility.

5 Conclusions

In this study, we have investigated the performances of OTFS modulation in GEO and LEO satellite-to-ground channels at sub-6-GHz and millimeter-wave bands with high mobility, and the MMSE-SD algorithm has been adopted to improve the BER performance. Using the 3GPP NTN-TDL channel models, we have compared the BER performances of OTFS modulation in various scenarios, under LoS and NLoS conditions. Because OTFS modulation can achieve full diversity in the delay-Doppler domain, we found that OTFS modulation performs better than OFDM in satellite-to-ground high-mobility communications, and that different terminal velocities do not have a significant impact on OTFS BER performance. The results showed that different scenarios do not have a significant impact on the BER performance of OTFS modulation in NLoS conditions, and that the MMSE-SD algorithm can achieve at least 2.3-dB gain compared with MMSE. The results also showed the feasibility of applying OTFS modulation in satellite-to-ground communications with high mobility.

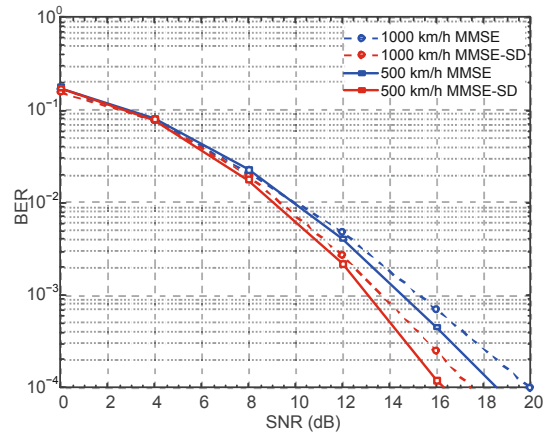


Fig. 9 BER performance of MMSE-SD and MMSE at the carrier frequency of 2.2 GHz in a dense urban scenario

BER: bit error rate; MMSE: minimum mean squared error; MMSE-SD: MMSE with successive detection

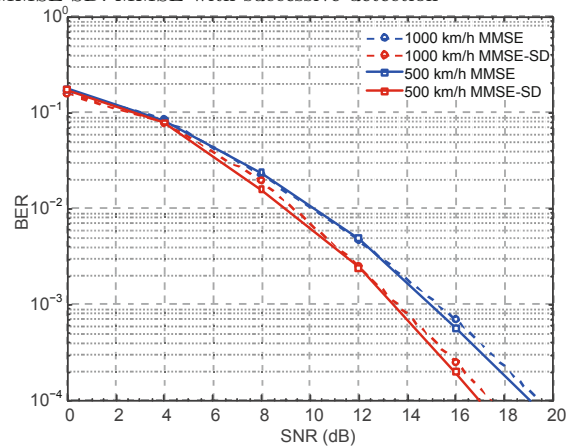


Fig. 10 BER performance of MMSE-SD and MMSE at the carrier frequency of 20 GHz in a dense urban scenario

BER: bit error rate; MMSE: minimum mean squared error; MMSE-SD: MMSE with successive detection

Contributors

Tianshi LI, Ruisi HE, and Haoxiang ZHANG designed the research. Tianshi LI, Bo AI, and Mi YANG designed the signal processing algorithm. Tianshi LI, Ruisi HE, and Haoxiang ZHANG conducted the simulations and drafted the manuscript. Zhangdui ZHONG helped organize the manuscript. Zhangdui ZHONG and Haoxiang ZHANG improved the simulations. Tianshi LI and Ruisi HE revised and finalized the paper.

Compliance with ethics guidelines

Tianshi LI, Ruisi HE, Bo AI, Mi YANG, Zhangdui ZHONG, and Haoxiang ZHANG declare that they have no conflict of interest.

References

- 3GPP, 2020. Study on New Radio (NR) to Support Non-terrestrial Networks. 3GPP TR 38.811 V15.3.0.
- Ai B, Molisch AF, Rupp M, et al., 2020. 5G key technologies for smart railways. *Proc IEEE*, 108(6):856-893. <https://doi.org/10.1109/JPROC.2020.2988595>
- Chen R, Yang WH, Xu H, et al., 2018. A 2-D FFT-based transceiver architecture for OAM-OFDM systems with UCA antennas. *IEEE Trans Veh Technol*, 67(6):5481-5485. <https://doi.org/10.1109/TVT.2018.2817230>
- Chen XM, Zhang S, Li QL, 2018. A review of mutual coupling in MIMO systems. *IEEE Access*, 6:24706-24719. <https://doi.org/10.1109/ACCESS.2018.2830653>
- Chen XM, Xue W, Shi HY, et al., 2020. Orbital angular momentum multiplexing in highly reverberant environments. *IEEE Microw Wirel Compon Lett*, 30(1):112-115. <https://doi.org/10.1109/LMWC.2019.2952975>
- Choi YS, Voltz PJ, Cassara FA, 2001. On channel estimation and detection for multicarrier signals in fast and selective Rayleigh fading channels. *IEEE Trans Commun*, 49(8):1375-1387. <https://doi.org/10.1109/26.939860>
- Fan BK, Li Y, Zhang RY, et al., 2020. Review on the technological development and application of UAV systems. *Chin J Electron*, 29(2):199-207. <https://doi.org/10.1049/cje.2019.12.006>
- Hadani R, Rakib S, Tsatsanis M, et al., 2017. Orthogonal time frequency space modulation. *IEEE Wireless Communications and Networking Conf*, p.1-6. <https://doi.org/10.1109/WCNC.2017.7925924>
- Hadani R, Rakib S, Kons S, et al., 2018. Orthogonal time frequency space modulation. <https://arxiv.org/abs/1808.00519>
- He RS, Ai B, Stüber GL, et al., 2018. Geometrical-based modeling for millimeter-wave MIMO mobile-to-mobile channels. *IEEE Trans Veh Technol*, 67(4):2848-2863. <https://doi.org/10.1109/TVT.2017.2774808>
- He RS, Schneider C, Ai B, et al., 2020. Propagation channels of 5G millimeter-wave vehicle-to-vehicle communications: recent advances and future challenges. *IEEE Veh Technol Mag*, 15(1):16-26. <https://doi.org/10.1109/MVT.2019.2928898>
- Jayaprakash A, Chen HZ, Xiao P, et al., 2019. Analysis of candidate waveforms for integrated satellite-terrestrial 5G systems. *IEEE 2nd 5G World Forum*, p.636-641. <https://doi.org/10.1109/5GWF.2019.8911721>
- Li B, Luan X, Si Y, et al., 2012. Selection of sub-carrier bandwidth in OFDM based mobile satellite communication. *IEEE Int Conf on Information Science and Technology*, p.798-801. <https://doi.org/10.1109/ICIST.2012.6221758>
- Lin WL, Wang HJ, Deng ZL, et al., 2020. State machine with tracking tree and traffic allocation scheme based on cumulative entropy for satellite network. *Chin J Electron*, 29(1):183-189. <https://doi.org/10.1049/cje.2019.06.024>
- Nimr A, Chaffi M, Matthe M, et al., 2018. Extended GFDM framework: OTFS and GFDM comparison. *IEEE Global Communications Conf*, p.1-6. <https://doi.org/10.1109/GLOCOM.2018.8647704>
- Papathanassiou A, Salkintzis AK, Mathiopoulos PT, 2001. A comparison study of the uplink performance of W-CDMA and OFDM for mobile multimedia communications via LEO satellites. *IEEE Pers Commun*, 8(3):35-43. <https://doi.org/10.1109/98.930095>
- Pfadler A, Jung P, Stanczak S, 2020. Pulse-shaped OTFS for V2X short-frame communication with tuned one-tap equalization. *24th Int ITG Workshop on Smart Antennas*, p.1-6.
- Raviteja P, Phan KT, Hong Y, et al., 2018. Interference cancellation and iterative detection for orthogonal time frequency space modulation. *IEEE Trans Wirel Commun*, 17(10):6501-6515. <https://doi.org/10.1109/TWC.2018.2860011>
- Raviteja P, Hong Y, Viterbo E, et al., 2019a. Practical pulse-shaping waveforms for reduced-cyclic-prefix OTFS. *IEEE Trans Veh Technol*, 68(1):957-961. <https://doi.org/10.1109/TVT.2018.2878891>
- Raviteja P, Phan KT, Hong Y, 2019b. Embedded pilot-aided channel estimation for OTFS in delay-Doppler channels. *IEEE Trans Veh Technol*, 68(5):4906-4917. <https://doi.org/10.1109/TVT.2019.2906357>
- Shen WQ, Dai LL, An JP, et al., 2019. Channel estimation for orthogonal time frequency space (OTFS) massive MIMO. *IEEE Trans Signal Process*, 67(16):4204-4217. <https://doi.org/10.1109/TSP.2019.2919411>
- Surabhi GD, Augustine RM, Chockalingam A, 2019. On the diversity of uncoded OTFS modulation in doubly-dispersive channels. *IEEE Trans Wirel Commun*, 18(6):3049-3063. <https://doi.org/10.1109/TWC.2019.2909205>
- Wang TJ, Proakis JG, Masry E, et al., 2006. Performance degradation of OFDM systems due to Doppler spreading. *IEEE Trans Wirel Commun*, 5(6):1422-1432. <https://doi.org/10.1109/TWC.2006.1638663>
- You X, Wang CX, Huang J, et al., 2020. Towards 6G wireless communication networks: vision, enabling technologies, and new paradigm shifts. *Sci China Inform Sci*, 64:110301. <https://doi.org/10.1007/s11432-020-2955-6>
- Zhang HY, Huang XJ, Zhang JA, 2019. Comparison of OTFS diversity performance over slow and fast fading channels. *IEEE/CIC Int Conf on Communications in China*, p.828-833. <https://doi.org/10.1109/ICCChina.2019.8855898>